The energy metabolic footprint of predictive processing in the human brain

André Hechler[1,2,*], Floris P. de Lange[3], Valentin Riedl[1,2]

[1] Department of Neuroradiology, Neuroimaging Center, Technical University of Munich, Munich, Germany

[2] Graduate School of Systemic Neurosciences, Ludwig-Maximilians-University, Munich, Germany

[3] Donders Institute for Brain, Cognition and Behaviour, Radboud University Nijmegen, Nijmegen, the Netherlands

*Corresponding author. Contact: andre.hechler@tum.de

Abstract

Neural activity is a highly energy-intensive process. In the human brain, signaling consumes up to 75% of the available energy resources with postsynaptic potentials as the largest factor. Visual processing is especially costly, with increases in energy consumption of up to 20% in the visual cortex. In recent years, vision has been cast as a constructive process, harnessing prior knowledge in a constant feedback loop of top-down prediction and bottom-up sensory input. Interestingly, sensory input that is in line with our predictions might be processed at lower energy metabolic cost. However, there is no evidence for this claim yet, possibly due to the scarcity of measures that quantify energy consumption in the human brain.

Here, we used a novel MR method measuring the cerebral metabolic rate of oxygen during sensory stimulation of visual sequences that varied in their predictability. Since predictive processing is driven by estimates of uncertainty, we assessed how confident subjects were in their knowledge of the underlying patterns. We found that processing predictable sequences steeply decreased in energetic cost with increasing confidence. Strikingly, these energetic effects were not limited to visual areas, summing up to a cortical difference of 13% between high and low levels of confidence. Furthermore, sequences deviating from expectations were energetically cheaper than predictable ones for low confidence levels, but costlier for high levels. These results speak for a major role of predictive processing in balancing the brain's energy budget and emphasize the impact of interindividual differences when learning predictive patterns.

Introduction

To produce the energy that fuels neural activity, the brain needs a steady supply of oxygen and glucose. Neural signaling is estimated to account for 75% of the brain's energy consumption in grey matter with 50% of that fraction going towards postsynaptic potentials (Howarth et al., 2012). The rate of energy consumption is strongly affected by sensory stimulation: In the visual cortex, up to 20% more energy is used during stimulation (Lin et al., 2010). Such effects cannot be reliably measured by conventional BOLD imaging, which is strongly driven by hemodynamic effects (Drew, 2019). While blood flow and energy consumption are tightly coupled at rest, the ratio differs across the cortex (Devonshire et al., 2012; Drew, 2022; Hyder, 2010) and is impacted by attentional state (Moradi et al., 2012) as well as stimulation duration (Moradi & Buxton, 2013). Addressing this problem, multiparametric quantitative BOLD imaging (mqBOLD; Blockley et al., 2013; Bright et al., 2019; Christen et al., 2012) provides direct access to energy metabolic processes by measuring the cerebral metabolic rate of oxygen on a voxel level (CMR_{O2}). CMR_{O2} has three key advantages for research on energy consumption: First, it represents the main resource of ATP production in the brain (Dienel, 2014; Harris et al., 2012) and is biologically interpretable. Second, it combines separate measurements of hemodynamics and blood (de-)oxygenation. This accounts for differences in neurovascular coupling, allowing the comparison and integration of CMR_{O2} across the brain. Third, due to the quantitative approach, CMR_{O2} can be analyzed in absolute values, enabling inference on conditions instead of contrasts while staying comparable between subjects.

Previous studies on the energetic cost of visual perception purely focused on stimulus characteristics, presenting simple or complex stimuli and limiting the analysis to the visual cortex (Griffeth et al., 2015; Lin et al., 2010). However, perception can be understood as a constructive process that heavily relies on prior knowledge from higher cognitive areas to interpret sensory input (Clark, 2013; de Lange et al., 2018; Teufel & Fletcher, 2020). The predictive coding framework posits that the brain is constantly optimizing a model of the world with the goal of minimizing the surprise of sensory observations (Rao & Ballard, 1999). Deviations from the model lead to error signals and subsequent model updating which are implemented in the brain as hierarchical feedback loops (Bastos et al., 2012; Walsh et al., 2020). A cornerstone of predictive processing is the extraction of spatial and temporal patterns to infer causes from incomplete observations and predict future events from past and current ones. The latter ability is exemplified by studies investigating statistical learning, where a sensory stream is generated from specific transitional probabilities. These provide a source of prediction after repeated exposure (Fiser & Lengyel, 2022; Turk-Browne et al., 2009, 2010). Studies using such a design revealed lower activation for expected compared to unexpected stimuli across conventional imaging modalities (Manahova et al., 2018; Richter et al., 2018; Stefanics et al., 2011). This is expected when understanding predictive coding as a theory of efficient coding (Chalk et al.,

2018; Quintela-López et al., 2022): By learning the patterns behind sensory input, our predictions can be optimized to the point where little to no error signals or changes to the internal model are necessary (for a mathematical derivation see Sengupta et al., 2013). However, there is no empirical evidence available that this results in reduced energy consumption.

In the present study, we extended an established visual statistical learning design with a multi-day training phase, maximizing consolidation of the underlying patterns. Additionally, we accounted for individual differences in the learning process by assessing participants' confidence in knowing the underlying patterns (Geurts et al., 2022; Meyniel, Sigman, et al., 2015; Sanders et al., 2016). Predictive processing theories heavily draw from Bayesian inference models where uncertainty about predictions has a major effect on perception (Yon & Frith, 2021). While statistical learning is based on continuous, partly implicit processes (but see Dale et al., 2012; Vadillo et al., 2016), a line of studies has shown that intermittent confidence ratings separate from the learning process reflect the statistical confidence of a Bayesian observer during the learning blocks (Bounmy et al., 2023; Meyniel, Schlunegger & Dehaene, 2015; Meyniel & Dehaene, 2017).

To summarize, we here used a MR-derived measure of oxygen consumption to study how predictive characteristics of external input and internal beliefs impact the brain's energy balance. We hypothesized that predictable stimuli are cheaper to process than unexpected stimuli and that this difference scales with subjective confidence in the predictable patterns. To preview our findings, the energetic cost of predictable input indeed decreased with confidence in both sensory and higher cognitive regions. Intriguingly, a general energetic advantage only emerged at high confidence levels.

Results

Confidence ratings and processing speed increase with repeated exposure to visual patterns

Prior to the scanning session, participants completed a three-day online training phase. They were presented with image sequences of everyday objects that either followed a deterministic pattern (predictable condition, P) or a random pattern (unpredictable condition, U) (Figures 1a and b). To ensure vigilance and gaze fixation, participants had to react to upside-down objects, which occurred irrespective of sequence predictability. Average accuracy exceeded 95% and neither accuracy nor reaction time differed between conditions (reaction time: $t(40)=-1.4$, $p=.17$; accuracy: $t(40)=1.51$, $p=.14$). Separate from the statistical learning blocks, we assessed the trajectory of learning both on an objective and a subjective scale. To this end, we presented participants with incomplete sequences and prompted them to choose the correct follow-up object. For each choice, we assessed confidence ratings as an indicator of uncertainty regarding knowledge of the underlying patterns (Figure 1c). Over the training days, confidence ratings increased for predictable visual sequences while they remained constant for unpredictable input (Figure 1d, left). We also saw an objective improvement in pattern

completion (Figure 1d, right) which was highly correlated with confidence (r=0.82, p<0.001). Since we did not provide any feedback, this suggests that participants were highly accurate in assessing their performance.

Directly prior to scanning, we included an additional task that aimed at detecting improvements in an implicit marker of learning. Similar to the training phase, we presented predictable and unpredictable sequences. Instead of performing the cover task, participants were instructed to react to the occurrence of a target object that was shown before each sequence. The target was randomly chosen from the upcoming objects, meaning it could be anticipated in the predictable condition. We found that participants detected predictable objects over 10% faster (median RT change=-10.75%, t=-5.7, p<0.001). Furthermore, this difference scaled with confidence ratings, meaning that confident subjects gained a stronger increase in processing speed (Figure 1e).

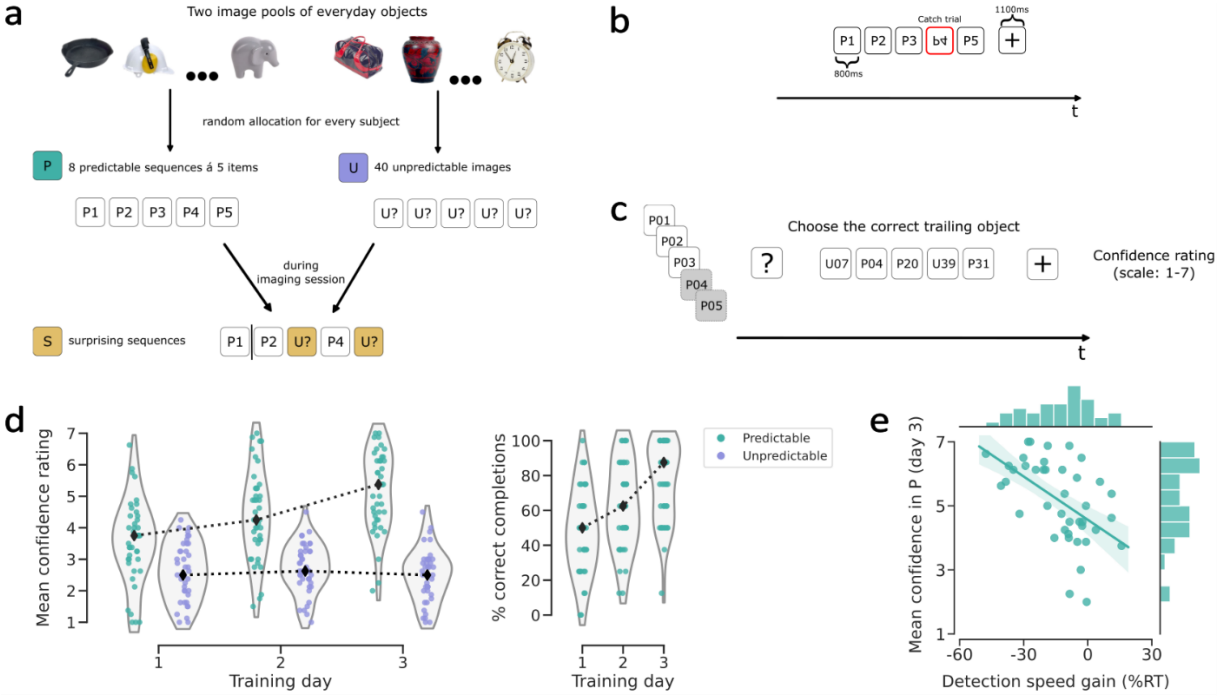

Figure 1. **a**. Experimental stimuli were sequences of five everyday objects. Predictable sequences (P) had consistent order and composition, unpredictable ones (U) were random. During MR acquisition, surprising sequences (S) composed of P and U were additionally shown. See Methods section for details. **b**. Stimulus presentation. Objects were shown sequentially and have no interstimulus interval. With a 10% chance, an image was horizontally flipped, and participants had to react with a button press. **c**. Sequence completion test after each training day. One to four images of a sequence were shown, and the correct trailing object had to be chosen from five options. This was followed by a confidence rating prompt. **d**. *Left*: Subject-wise average confidence ratings following respective training days. Black lines and markers indicate day-wise sample medians. *Right*: Percentage of correctly chosen trailing images in the completion test. Averaged completion percentage is in steps of 12.5% because eight sequences were tested per day. **e**. Results of separate object detection task. Detecting a predictable compared to an unpredictable target was significantly quicker for participants with high confidence (r=-0.54, p<0.001). Negative values indicate faster reactions for predictable objects.

The interaction of predictability and confidence drives energy consumption

For our main analysis, we first created voxel-wise brain maps of CMR_{O2} from our MR and blood sampling data (Figure 2a and Methods). We then averaged condition-wise CMR_{O2} values for every subject within 400 functional regions as defined by the Schaefer parcellation (Schaefer et al., 2018).

This was done to control for voxel-level noise and to differentiate sensory from higher cognitive regions. Prior to analyzing the imaging data, we tested for potential confounding effects of the cover task. Unlike during the training phase, we found differences between conditions (repeated measures ANOVA: $F(2,80)=4.44$, $p=0.015$). Post-hoc tests showed that participants reacted most quickly to predictable items (Figure 2b). This is surprising, given the independence of the cover task from sequence predictability and the absence of reaction time differences in the training phase. Consequently, we controlled for these effects in the following analyses.

In contrast to conventional GLM analyses, our aim was not to localize regions of maximum effect, but to assess net energetic changes on a larger scale. As argued previously, evoked activity extends far beyond local peaks which can limit results to the "tip of the iceberg" (Noble et al., 2022, 2023). To address this, we analyzed metabolic effects on the level of functional networks. We used a whole-brain linear mixed model with predictors of condition, confidence, functional network and reaction time in the cover task (Methods). Essentially, this model allowed us to explain regional CMR_{O2} as a linear combination of predictability and confidence, with separate regressors for six functional networks while accounting for confounding effects of reaction time. The random term of the model addresses subject-specific baselines of CMR_{O2} on which the fixed terms are added. Confidence values correspond to the condition-wise average after the last training day, and we used ratings from the predictable sequences for the surprising condition. All resulting model estimates are relative to the reference categories of the respective predictors: We used the visual network and the predictable condition. Importantly, since CMR_{O2} values are quantitative, the model parameters for the reference levels can be interpreted without referring to a contrast estimate. Significant differences of surprising and unpredictable sequences compared to predictable ones are indicated by a significant parameter estimate for non-reference predictor levels.

We first confirmed that our model significantly improves upon a null model that lacks the experimental variable ($BF_{log}=131.51$; $X^2(42)=552.6$, $p<0.001$). Table 1 includes an overview of all significant predictors and the full model results are provided in the supplement. The intercept of 136.33 represents the grand average CMR_{O2} across subjects and conditions, in units of µmol O_2/min/100g. Validating our approach, this is well within the range of 120-160 usually reported for healthy human subjects (summarized in Xu et al., 2009, see also Christen et al., 2012; Göttler et al., 2019). With respect to our main research question, we found no main effect of condition, but a significant interaction between condition and confidence. This means that, while energy consumption did not differ between levels of predictability per se, the conditions were differentially affected by confidence levels. Overall, CMR_{O2} decreases with confidence (denoted by the negative estimate for the reference category) but this effect is offset in the surprising condition. The linear combination of these parameters is visualized in Figure 2e (for uncertainty of these estimates refer to Table 1). As the

reference category corresponds to the predictable condition, our results show a steep decrease of energetic cost with confidence for predictable sequences. Interestingly, this effect was not significantly different for unpredictable sequences, suggesting that confidence impacted energetic cost even in the face of objectively random stimulation. However, the corresponding parameter estimate showed a quantitative trend towards a weaker effect of confidence.

High confidence reduces energy consumption across the whole cortex

Interestingly, while the functional networks differed in their CMR_{O2} baseline, the interaction between predictability and confidence was largely consistent across the cortex. The control network is a notable exception: Here, the decrease of CMR_{O2} with confidence was significantly weaker than in the other networks. Regarding unpredictable sequences, the control network showed another unique deviation. Irrespective of confidence levels, its energy consumption was significantly higher than in the other conditions.

Given that the interaction of condition and confidence was found across networks, we evaluated the net effect on the whole cortex. To achieve this, we used the significant model parameters of confidence and network to calculate the predicted CMR_{O2} for low (5^{th} percentile), average (50^{th} percentile) and high (95^{th} percentile) confidence. Since CMR_{O2} is a rate of consumption relative to a tissue mass of 100g, we scaled the predicted energy consumption to the gray-matter mass of the respective networks (Methods). Strikingly, our data suggest that high confidence reduces cortical energy consumption by 13.25% (CI: [0.34; 26.16]) relative to low levels of confidence (Figures 2d).

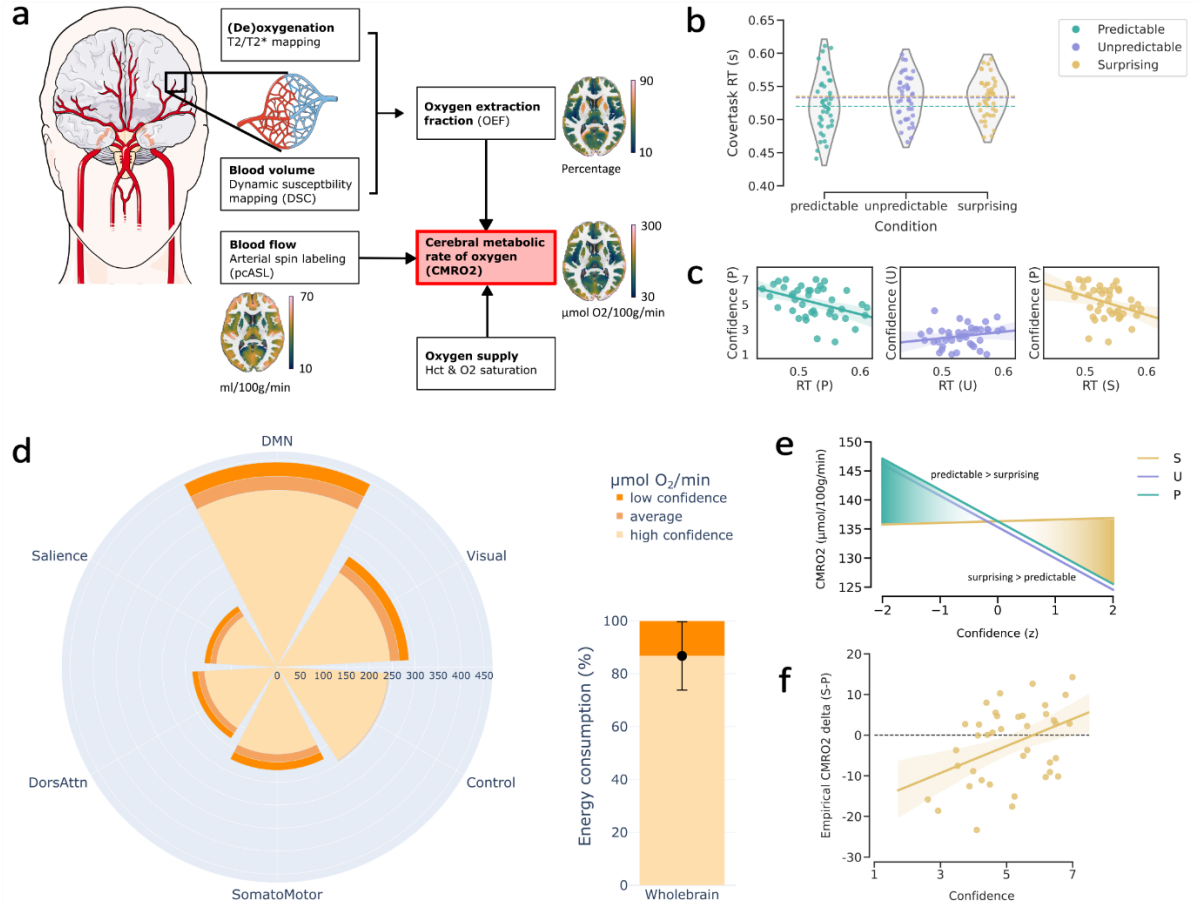

Figure 2. **a**. Flowchart depicting the workflow of CMR_{O2} calculation from experimental data*. Parameter maps show group averages in cerebral grey matter. Details are described in the method section. **b**. In the cover task, participants reacted significantly quicker to predictable than surprising objects (t(*40*)=-2.9, p_{FWE}=0.017) with a trend in the same direction compared to unpredictable objects (t(*40*)=-2.24, p_{FWE}=0.091). Points show subject-wise averages across the scanning session and dashed lines indicate condition-wise medians. **c**. Condition-wise correlations between confidence ratings and reaction time in the cover task during scanning. We found a significant negative association for the predictable condition (r=-0.42, p_{FWE}=0.018). The effect was similar for the surprising condition but did not survive FWE correction (r=-0.36, p_{FWE}=0.066). **d**. *Left*: Oxygen consumption per minute (scaled to network gray-matter mass) as predicted by the significant model terms of network and confidence. Low, average and high confidence correspond to the 5th, 50th and 95th percentile of z-scaled confidence ratings. *Right*: Predicted relative energy consumption for subjects with high confidence compared to low confidence, summed over all networks. The black error bar indicates the 95th confidence interval of estimated energy consumption in high confidence subjects based on the confidence interval of the model parameter (see Methods). **e**. Predicted CMR_{O2} across confidence levels for the reference network (Visual). Shaded areas indicate whether predictable sequences (green) or surprising sequences (yellow) are more costly. Note that the slope for predictable and unpredictable entirely overlaps according to our model. The regression lines are slightly offset for visualization purposes. **f**. Cortical CMR_{O2} difference between surprising and predictable sequences is explained by confidence (linear regression controlling for reaction time: $R^2_{partial}$=.18, t(*40*)=2.92, p=0.005). Data shown are subject-wise cortical CMR_{O2} differences between surprising and predictable sequences in the experimental data. **Visualizations of head and vessels were created using Servier Medical Art, provided by Servier, licensed under a Creative Commons Attribution 3.0 unported license*

Predictor level	Predictor (only significant§)	Estimate (in µmol O2/min/100g)	95% CI	p-value
Main effect*	Intercept	136.33	128.84 – 143.83	<0.001
	confidence	-5.39	-9.88 – -0.9	0.019
	reaction time	-4.84	-7.73 – -1.95	0.001
	network[control]	10.91	7.28 – 14.54	<0.001
	network[DMN]	8.26	5.08 – 11.43	<0.001
	network[SomMot]	-11.81	-15.08 – -8.54	<0.001
	network[salience]	-17.67	-21.37 – -13.96	<0.001
Interaction	condition[S]*confidence	5.67	-2.25 – 12.45	0.026
	condition[U]*confidence	5.10	-0.27 – 12.94	0.174§
	condition[U]*reaction time	3.12	0.16 – 6.08	0.039
	condition[U]*network[control]	6.51	0.8 – 12.21	0.025
	confidence*network[control]	5.03	1.7 – 8.35	0.003

Table 1. Significant predictors estimated by a robust linear mixed model with the following formula (following R conventions): condition*confidence*network + condition:reaction_time + (1|subject/condition). Estimates reflect absolute CMR_{O2} values and can be interpreted as a predicted change in energy consumption for a given change in (standardized) predictors. Non-significant predictors are omitted for brevity. We provide the full model output in the supplement. *Parameters are based on these reference categories: condition[predictable] and network[visual] §Additional inclusions due to importance for experimental interpretation

Relative cost of surprising input is a function of decreasing cost of predictable input

As non-quantitative imaging methods are limited to contrast-based analyses, prediction error activity is often formalized as a relative increase in activity for surprising over predictable input. Since our quantitative data resolves the cost of individual conditions, it informs us about the origins of relative effects. Looking at the condition-wise slopes (Figure 2e), our model suggested that relative prediction error activity emerges as a function of the decreasing cost of predictable input. We tested this assumption on our empirical data, regressing the difference between CMR_{O2} in the surprising and predictable condition against confidence. As expected, prediction error activity emerged at high levels of confidence (Figure 2f) across the cortex. Interestingly, the opposite was true for low levels of confidence and both conditions had similar energetic cost at slightly above average confidence.

Cover task reaction times play in major role for energy consumption

According to our model, reaction times in the cover task had a general effect on cortical energy consumption, with a magnitude similar to the effect of confidence. The slower subjects reacted to the

upside-down stimuli, the lower their energy consumption was across conditions (Table 1). However, this effect was significantly weaker in the unpredictable condition. Since confidence was central to the effect of predictability on energy consumption, we wondered if it also explains differences in reaction time. We therefore correlated confidence ratings and reaction times for each condition separately.

Interestingly, reaction times decreased with confidence in the predictable and the surprising condition, although the latter association did not survive correction for multiple comparisons (Figure 2c). Although tentative, this pattern has an intriguing implication for the energy metabolic effects: While more confident subjects used less energy for predictable input, they also reacted quicker in the cover task, which in turn increased energy consumption. This led us to ask the question whether these effects even out according to our model. We recalculated the net cortical energy consumption with opposing effects of reaction time (methods). While the trend of a cortical CMR_{O2} decrease persisted (8.27%, CI: [-5.46; 22.03]), we found no significant evidence when factoring in opposing effects of reaction time.

Discussion

In the present study, we quantified the metabolic cost of processing visual sequences under different levels of objective and subjective predictability. According to the predictive coding framework, humans build a predictive model of the world that is updated when deviations are encountered (Rao & Ballard, 1999). Expected visual stimuli lead to weaker error signaling and model updating across processing hierarchies of the cortex (Bastos et al., 2012; Walsh et al., 2020). It has been argued that these predictive models balance accuracy and complexity (Friston, 2010). This might promote the minimization of energy usage in the brain (Sengupta et al., 2013). Due to the limited availability of in-vivo metabolic imaging methods, this assumption has never been tested.

We show that cortical energy consumption is driven by the interaction between the objective predictability of visual input and subjective confidence in knowing the patterns. When presented with highly predictable input, energy consumption decreased with increasing confidence, up to a cortical difference of 13 percent. As a consequence, perceiving surprising input became more costly in comparison. These effects were remarkably consistent across the cortex, with only the control network showing slight deviations from the system-level effect. High confidence was also linked to quicker detection of predictable stimuli. In summary, we found that predictable patterns promote behavioral improvements and concurrent energy metabolic reductions.

Energy metabolism and efficiency

When formulating biologically realistic models of brain function, accounting for resource constraints is crucial (Roberts et al., 2014). Healthy brain function relies on constant oxygen and glucose delivery and shortages can have severe consequences ranging from cognitive deficits to cell death (Lee et al., 2020; Warren & Frier, 2005). Interestingly, the brain seems to be optimized for

efficiency, from the firing patterns of neurons to the architecture of functional networks (Yu & Yu, 2017; Zhou et al., 2022). In related cognitive research, it has been argued that learning is an efficient process that maximizes performance while minimizing cost (Commins, 2018). These lines of research can be unified from an information-theoretic perspective: Akin to training algorithms in machine learning, the brain might aim to optimize behavioral accuracy while minimizing the complexity of internal representations (Zénon et al., 2019). This notion has been generalized under the Free Energy Principle (Friston, 2010): Humans build an internal model of the world that is continuously updated with new information, balancing model accuracy with model complexity. Assuming that the brain represents this model, the efficiency of the model might extend to the energetic efficiency of the underlying neural activity (Sengupta et al., 2013). Computational studies using neural networks are in support of this hypothesis: Networks trained to minimize their activity in a sequence prediction task developed predictive architectures (Ali et al., 2022) and predictive learning algorithms were expressed as energy-minimization algorithms (Luczak et al., 2022). Despite these theoretical and computational underpinnings, no direct evidence is available that predictive processing leads to metabolic efficiency.

The role of subjective confidence during statistical learning

The ability to extract transitional probabilities from sequential stimulation is often termed statistical learning and has a rich tradition in cognitive research (Schapiro & Turk-Browne, 2015). Previous work focused on the assumed automaticity of the learning process, which can happen in the absence of intention or awareness (Alamia et al., 2016; Turk-Browne et al., 2005). However, recent work showed that, while implicit processes are a prerequisite, explicit knowledge can be acquired in parallel (Batterink et al., 2015; Dale et al., 2012). Blurring the lines further, Conway (2020) argued that most designs studying the learning process of transitional probabilities tap into the same underlying process. However, there is evidence for a difference in the neuroanatomical substrates of implicit and explicit statistical learning, so comparisons between studies should be drawn with care (Aizenstein, 2004). Recently, it has been suggested that a general Bayesian inference process underscores all probabilistic computation (Fiser & Lengyel, 2022). Consequently, instead of addressing a specific paradigm, the current work used streams of visual sequences as a tool to elicit probabilistic learning.

By including confidence ratings, we addressed a major parameter of Bayesian inference: Uncertainty (often referred to by its inverse, *precision*). Both perception and decisions are subject to uncertainty, stemming from both external sources (e.g. the visibility of a stimulus) and internal sources (e.g. noise in neural transmission) (Bach & Dolan, 2012). These sources have downstream effects on the identification of rules in our environment or the prediction of likely outcomes of a decision. Furthermore, while Bayesian inference is a powerful model of human cognition, individuals often deviate from the idealized performance (Acerbi et al., 2014; Beck et al., 2012). These lines of research suggest that considerable interindividual differences are to be expected when submitting a group of

participants to the same task. To account for this variance, we used confidence ratings as a proxy for individual uncertainty.

The exact interpretation and implementation of confidence ratings is still debated. Previously, it has been defined as the posterior probability that a choice is correct, given the evidence (Pouget et al., 2016). For a statistically precise estimate, a neural representation of probability distributions is needed, an assumption that has been called into question (Koblinger et al., 2021). A promising explanation are probabilistic population codes (Knill & Pouget, 2004). Under this model, neurons are sensitive to different expressions of internal or external variables, adjusting their firing pattern or frequency according to the similarity of the stimulus to their preferred values. A population of neurons can then serve as a probability distribution over possible values of the variable (for a review of the evidence see Ma & Jazayeri, 2014). In this context, confidence ratings provide a summary statistic over this distribution, indicating the spread of the probability distribution around the central tendency (Meyniel, Sigman & Mainen, 2015). However, multiple alternative explanations have been developed, ranging from approximations to non-Bayesian accounts of confidence (Adler & Ma, 2018). Nevertheless, most formulations agree that some form of confidence-weighting is central to the human inference process.

The effect of subjective confidence on energetic cost

Our results confirm that confidence determines energy consumption during varying levels of objective predictability. The link between confidence and brain activation during probabilistic learning has been investigated in a previous line of studies using conventional BOLD (Bounmy et al., 2023; Meyniel, Schlunegger & Dehaene, 2015; Meyniel & Dehaene, 2017). Three caveats apply when comparing these studies to our results. First, we presented long blocks with stable transitional probabilities, while the underlying parameters were volatile in their design. Second, local BOLD effects do not necessarily correspond to energy consumption (Drew, 2019), especially when extending the analysis above local peaks as in our case. Lastly, our data represents an average of multiple minutes of visual input. Transient brain responses as revealed by BOLD analyses may not correspond to the net efficiency of a given neural process. Consequently, our data is reflective of the aggregate cost of continuous precision-weighted updating.

The aforementioned studies found that BOLD activity decreased with confidence while it increased with surprise in various areas. They also report results for regions most sensitive to precision-weighted updating: Here, surprising input elicited higher signal across confidence levels. In contrast, we found that predictable input leads to higher energy consumption than surprising input for low confidence, while the inverse was true for high confidence. Furthermore, the cost of surprising input did not change with confidence in our data. A possible explanation is the length of the presentation blocks in our study: While deviations from the learned sequences were initially surprising, participants

might have learned the increased variance of the presentation. This would make the surprising sequences more akin to sequences of intermediate (probabilistic) predictability. In line with this argument, humans have been shown to track changes in environmental statistics, discounting previous observations (Beierholm et al., 2020; Maheu et al., 2022). In this case, confidence ratings from the previously predictable condition would have no lasting effect on the ”surprising” condition.

Nevertheless, we still reproduced the classical pattern of higher cost for surprising compared to predictable input. In our data, this effect only emerged at high confidence levels due to the decreasing cost of predictable input. This addresses the arbitration between two potential processes behind prediction errors: Surprise enhancement assumes that surprising stimuli evoke stronger signals while expectation suppression assumes decreased signals for predictable input (Feuerriegel et al., 2021; Manahova et al., 2018). From the perspective of energy consumption, our data is suggestive of expectation suppression as the source of relative prediction errors. This contrasts with results from BOLD and EEG studies, where evidence for surprise enhancement is stronger (reviewed in Feuerriegel, Vogels & Kovács (2021)).

Interestingly, the effect of confidence on cortical cost was not significantly different between predictable and objectively random input. Since we gave no feedback during the sequence prediction task, it is possible that participants thought they detected a pattern in the random sequences. This is supported by the low, but far from minimal confidence ratings for unpredictable sequences during training. Humans tend to perceive structure even in random sequences (Huettel et al., 2002) which might drive perceptual inference in the absence of feedback. Future studies are needed to examine to which extent the effect of precise priors is independent of their objective accuracy. We also found that reaction times in the cover task increase with confidence during predictable and surprising sequences. This indicates that highly confident subjects improved their performance in a concurrent, but unrelated task. A tentative interpretation is that participants shifted their resources from model updating to lower-level perception of the objects' orientations. Under this assumption, the brain does not aim to decrease energy consumption per se, but rather reassigns resources dynamically under the constraints of energy availability (Christie & Schrater, 2015).

Energetic changes on a cortical level

In summary, our results show that an experimental manipulation as seemingly small as a change to transitional probabilities can lead to large differences in energy consumption. Surprisingly, these effects were highly consistent over the cortex, affecting both sensory and higher cognitive networks. Importantly, our study does not speak to the functional specificity of these energetic changes. Rather, we provide evidence for the net effect of perceptual inference on the cortex. The widespread changes in energy metabolism are in line with recent accounts of brain function as a highly integrated system (Pessoa, 2023). The focus on localization in neuroimaging research might have been

supported by traditional mass-univariate analyses, which restrict the view of the brain to the "tip of the iceberg" (Noble et al., 2022, 2023). Specific to predictive processing, a recent meta-studied found a brain-spanning prediction network that encompassed functionally connected regions across the brain (Ficco et al., 2021). Furthermore, a recent preprint reported representations of prior information across all levels of processing in the mouse cortex (Findling et al., 2023). In line with these works, we propose that the efficiency of a highly integrative system is best evaluated over a correspondingly large spatial extent.

Oxidative versus glycolytically driven energy metabolism

Lastly, a recent paper developed an integrative framework drawing a direct link between predictive processing and differential patterns of BOLD, CMR_{O2} and CMR_{Glc} (the cerebral metabolic rate of glucose) (Theriault et al., 2023). The authors argue that the ratio between ATP-yielding metabolites differs between bottom-up prediction errors and top-down predictions: Prediction errors rely on fast and flexible ATP generation via non-oxidative glycolysis, while prediction is based on the more efficient but less flexible oxidative phosphorylation. Importantly, the BOLD signal is driven by blood flow, which indicates oxygen availability but not necessarily oxygen consumption (Fox et al., 1988). As blood flow is more closely related to glucose use than oxygen use, BOLD is a better reflection of CMR_{Glc} than CMR_{O2} (Raichle & Mintun, 2006). It follows that, on the one hand, our CMR_{O2} data might be less sensitive to changes in error signaling but on the other hand, it could unveil prediction-related changes that BOLD does not capture. Future studies could dig deeper into these assumptions with the aim of providing a complete picture of the energy metabolism of the brain during predictive processing.

Methods

Participants

We recruited 44 participants including students, doctoral researchers, clinic staff and the general population of Munich. The sample size was based on a-priori analysis, aiming to detect at least a medium effect size (d>=0.5, alpha=0.05, beta=0.9). All participants took part in a familiarization MRI session (20 minutes), an online training phase over three days and the main MRI session (70 minutes) on the day after training completion. Two participants were excluded due to technical problems during data acquisition. One further subject was excluded from analysis because their data indicated that the training phase was not properly performed: The same button was pressed for every confidence rating prompt and performance was still at chance level after the full training phase. The remaining 41 participants (18 female, age [mean(std)] = 27(3.9)) were included for all analyses. The study was approved by the ethics board of the Technical University of Munich (TUM), and we acquired written informed consent from all participants.

Visual stimuli

We selected 224 full-color images of everyday objects from a larger image set (Brady et al., 2008). The stimuli were chosen to be maximally homogenous regarding salience, e.g., by excluding food items and bright colors. All allocations of stimuli to subjects and conditions were random. Figure 1a visualizes the creation of the visual streams. A pool of 80 images was generated for every subject, with half assigned to the predictable condition and the other half to the unpredictable condition. Based on these images, eight predictable sequences were created for every subject. These objects could only occur in the sequence and position determined during stimulus creation. For the unpredictable condition, a starting set of eight sequences was created. After all were presented during the training or scanning phase, eight completely new sequences were randomly created for every repetition. Consequently, these objects never occurred in the same sequence or position, but the total number of occurrences was the same as for predictable objects. Lastly, only for the scanning phase, half of the predictable sequences and half of the unpredictable objects were combined into surprising sequences. Predictable sequences formed the basis but had one to three objects between position two and five replaced with a random object from the unpredictable condition. The first object was always unchanged to trigger conditional predictions based on the learned transition probabilities.

Experimental design

Implementation. We used Psychopy (Peirce et al., 2019) to implement the design. The online training sessions were realized using pavlovia.org, where Javascript-translated Psychopy experiments can be run online with millisecond precision (Bridges et al., 2020; Sauter et al., 2020).

Main task. We presented participants with continuous visual streams based on the described object sequences. Each stimulus was presented for 800ms with no inter-stimulus interval within sequence and a 1100ms fixation cross between sequences. When all unique sequences of a condition were shown, their order was reshuffled for continued presentation with the constraint that objects (or sequences) could not appear twice in a row. This was done to minimize confounding effects of repetition suppression. To ensure fixation and concentration, participants were instructed to quickly react to occurrences of upside-down objects. These appeared with a probability of 10%, independent of condition.

Training phase. Over the course of three days prior to the main scanning session, participants followed an online implementation of the main design. This phase only included the predictable und unpredictable sequences. We instructed every participant to perform the training in a quiet environment without distractions. Stimulation blocks lasted 20 minutes per day, with a break of one minute after 10 minutes. Instructions were shown on screen before the stimulation began and the first day included a five-minute familiarization block with on-screen feedback regarding cover-task button presses. The instructions stressed the importance of the cover task, but also noted that questions regarding the order of objects in a sequence would follow each training day. During this task,

participants saw eight incomplete sequences (the first one to four objects were shown) for both conditions (to keep image familiarity the same across conditions). After every sequence, participants chose what they assumed would be the correct trailing object from five options and gave a confidence rating on a scale of one to seven. No feedback was given regarding performance and no information on the underlying conditions was disclosed.

Imaging phase. During scanning, stimuli were presented against a grey background and subtended 4° of visual angle. Each condition was presented for three long blocks, during a pcASL sequence (6 minutes), a T2* sequence (5.5 minutes) and a DSC sequence (2.5 minutes). The order was randomized, although a condition could not occur three times in a row. We left breaks of one minute between each consecutive sequence. During the T2 sequence, there was no experimental stimulation. Per condition, a total of 169 object sequences over a stimulation time of approximately 14 minutes were presented. Before every scanning sequence, a reminder regarding the cover task was shown on screen. Additionally, participants got feedback on their mean reaction time after each sequence to promote attentiveness and motivation. We disclosed no information regarding the sequence patterns and the imaging session included no sequence completion test.

Object detection task. On the day of the imaging session, prior to entering the scanner room, participants performed an object detection task on a laptop. The presentation format followed the specifications of the main task, except for transitions between sequences. We presented eight unpredictable (reshuffled) and eight predictable (as learnt) sequences in random order. Prior to every sequence, a target object from the following sequence was shown. An onscreen prompt instructed participants to react as quickly as possible to the presentation of the target image by pressing the Arrow Up button. During the task, the target image was presented for five seconds. To allow for anticipation, it could only match positions two to five of the following sequence.

MRI acquisition

For CMR_{O2} mapping, the following sequences were acquired:

- Multi-echo spin-echo T2 mapping: 3D gradient spin echo (GRASE) readout as described previously (Kaczmarz et al., 2020), 8 echoes, TE1 = ΔTE = 16ms, TR=251ms, α=90°, voxel size 2x2x3.3mm^3, 35 slices. T2 data was acquired once per subject, without any task.
- Multi-echo gradient-echo T2* mapping: As described previously (Hirsch et al., 2014; Kaczmarz et al., 2020), 12 echoes, TE1 = ΔTE = 5ms, TR=2229ms, α=30°, voxel size 2x2x3mm^3, gap 0.3mm, 35 slices. T2* was acquired for all conditions.
- Dynamic susceptibility imaging (DSC): As described previously (Hedderich et al., 2019). Injection of gadolinium-based contrast agent as a bolus after 5 dynamic scans, 0.1ml/kg (maximum: 8ml per injection, 16ml per session), flow rate: 4ml/s, plus 25ml NaCl. Single-shot GRE-EPI, EPI factor 49, 80 dynamic scans, TR = 2.0s, α=60°, acquisition voxel size 2x2x3.5mm^3,

35 slices. To stay within the limits of a full clinical dosage (16ml), we acquired DSC in two conditions only: Predictable and unpredictable. Processing of the data in the surprising condition used DSC from the predictable condition.

- Pseudo-continuous arterial spin labeling (pcASL): As described previously (Alsop et al., 2015), and implemented according to (Göttler et al., 2019; Kaczmarz et al., 2020). PLD 1800ms, label duration 1800ms, 4 background suppression pulses, 2D EPI readout, TE=11ms, TR=4500ms, α=90°, 20 slices, EPI factor 29, acquisition voxel size 3.28x3.5x6.0mm^3, gap 0.6mm, 30 dynamic scans including a proton density weighted M0 scan. ASL was acquired for all conditions.

Prior to data acquisition, a venous catheter was placed by a medical doctor through which blood samples were taken and sent to our in-house clinical chemistry laboratory. Creatinin values were analyzed as an indicator of healthy kidney function and contrast agent was only applied for subjects below a threshold of 1.3. No subject exceeded this value. Hemoglobin and hematocrit were requested and used in modelling of CMR_{O2}. Finally, arterial oxygen saturation was measured via a pulse oximeter (Nonin 7500FO, Nonin Medical B.V., The Netherlands).

MRI data processing

To calculate CMR_{O2}, the following parameters were integrated and derived as described below: The oxygen content of blood (O_2 saturation and Hematocrit), the flow of blood (CBF), and the relative oxygen extraction (OEF). The processing of the quantitative parameter maps was performed with in-house scripts in MATLAB and SPM12 (Wellcome Trust Centre for Neuroimaging, UCL, London, UK). T2* images were corrected for macroscopic magnetic background gradients with a standard sinc-Gauss excitation pulse (Baudrexel et al., 2009; Hirsch & Preibisch, 2013). Motion correction was performed using redundant acquisitions of k-space center (Nöth et al., 2014). R2' maps are derived from T2 and T2* images and yield the transverse, reversible relaxation rate that is dependent on the vascular dHb content (Blockley et al., 2013, 2015; Bright et al., 2019). However, confounds from uncorrectable strong magnetic field inhomogeneities at air-tissue boundaries, iron deposition in deep GM structures as well as white matter structure need to be considered (Hirsch & Preibisch, 2013; Kaczmarz et al., 2020). The cerebral blood volume (CBV) was derived from DSC MRI via full integration of leakage-corrected ΔR2*-curves (Boxermann, J.L., Schmainda, K.M., Weisskoff, R.M., 2006) and normalization to a white matter value of 2.5% (Leenders et al., 1990) as described previously (Hedderich et al., 2019; Kluge et al., 2016). From R2' and CBV parameter maps, the oxygen extraction fraction (OEF) was calculated (Christen et al., 2012; Hirsch et al., 2014; Yablonskiy & Haacke, 1994). CBF maps were calculated from pcASL data, based on average pairwise differences of motion-corrected label and control images and a proton-density weighted image.

For each subject and condition, we calculated CMR_{O2} in a voxel-wise manner by combining all parameter maps via *Fick's principle*

$$\mathbf{CMR_{O2} = OEF \cdot CBF \cdot Ca_{O2}}$$

where Ca_{O2} is the oxygen carrying capacity of hemoglobin and was calculated as $Ca_{O2} = 0.334 \cdot Hct \cdot 55.6 \cdot O_2sat$, with O_2sat being the oxygen saturation measured by the pulse oximeter (Bright et al., 2019; Y. Ma et al., 2020) and Hct representing Hematocrit as measured by blood sampling prior to scanning. CBF was upscaled by 25% to account for systematic CBF underestimation due to four background-suppression pulses (Garcia et al., 2005; Mutsaerts et al., 2014). All parameter maps of each individual subject were registered to the first echo of their multi echo T2 data.

For statistical analysis of CMR_{O2}, we only included voxels with a grey matter probability of > 0.5. Furthermore, the images were masked using an intersection mask to exclude voxels with excessive susceptibility, indicative of artefacts (T2 and T2* > 120ms, R2' > 9ms) and voxels with biologically unlikely CBF (> 90 ml/min/100g) or OEF (> 90%).

Statistical analysis

Mixed models. We used robust linear mixed models as implemented in the R package robustlmer (Koller, 2016) to minimize the effect of outliers. This method uses the Huber loss function, which is quadratic for small differences, but linear for large differences. The random model term was used to specify conditions as repeated (nested) measurements within subjects. Consequently, our model estimated a subject-wise CMR_{O2} baseline for each condition. The fixed effects included a three-way interaction of condition, confidence and network as well as a two-way interaction of condition and reaction time in the covertask. Confidence values were based on the average condition-wise ratings after the last training day. Since surprising sequences were based on predictable ones, we assigned the same confidence ratings.

The input to our model were condition-wise regional CMR_{O2} values, obtained by the median voxel value within 400 functional areas (100 for model replication) as defined by the Schaefer parcellation (Schaefer et al., 2018). 30 of the 400 areas, mainly in the temporal pole and orbitofrontal cortex, had to be excluded from the analysis. This was due to susceptibility artefacts in the R2' maps, leading to signal dropout in these regions. The limbic network is therefore not covered by our model. Across subjects and areas, a total of 45507 observations entered the model estimation. We z-standardized the behavioral predictors and left the outcome CMR_{O2} values unchanged. For model estimation, we chose the predictable condition and the visual network as reference categories. A significant reference effect in the absence of significant parameter estimates for other categories means that the effect of the predictor does not vary across categorical levels. This also means that a significant effect for a non-reference category level has to be interpreted in relation to the main effect. Finally, we compared our model to a null model without the condition predictor using the performance

package (Lüdecke et al., 2021) for standard mixed models as implemented in lme4. Since the model outcome represents absolute CMR_{O2}, parameter estimates can be interpreted as the predicted change in energy cost for a given change in standardized predictors.

Model-based CMR_{O2} cost predictions. For model-based predictions, we added the corresponding parameter estimates as described in the results. Total CMR_{O2} was therefore calculated as the sum of the intercept (the sample baseline in the visual network), the network main effect (the difference of the network baseline from the intercept) and the main effect of confidence. We calculated the predicted cortical CMR_{O2} for weakly confident (5^{th} percentile, confidence(z)=-1.96), average (50^{th} percentile, confidence(z)=0) and highly confident (95^{th} percentile, confidence(z)=1.96) subjects. The outcome was then scaled to the grey matter mass of each network in MNI space, approximated by grey matter voxel count multiplied by a tissue mass of 0.0014 gram per cubic millimeter (Barber et al., 1970; IT'IS Foundation, 2022). Finally, predicted CMR_{O2} was summed over networks to obtain cortical values. We repeated this procedure for the 5^{th} and 95^{th} percentile of the confidence parameter estimate (Table 1) to obtain an upper and lower bound of the predicted energy cost.

References

Acerbi, L., Vijayakumar, S., & Wolpert, D. M. (2014). On the Origins of Suboptimality in Human Probabilistic Inference. *PLoS Computational Biology*, *10*(6), e1003661. https://doi.org/10.1371/journal.pcbi.1003661

Adler, W. T., & Ma, W. J. (2018). Comparing Bayesian and non-Bayesian accounts of human confidence reports. *PLOS Computational Biology*, *14*(11), e1006572. https://doi.org/10.1371/journal.pcbi.1006572

Aizenstein, H. J. (2004). Regional Brain Activation during Concurrent Implicit and Explicit Sequence Learning. *Cerebral Cortex*, *14*(2), 199–208. https://doi.org/10.1093/cercor/bhg119

Alamia, A., Orban de Xivry, J.-J., San Anton, E., Olivier, E., Cleeremans, A., & Zenon, A. (2016). Unconscious associative learning with conscious cues. *Neuroscience of Consciousness*, *2016*(1). https://doi.org/10.1093/nc/niw016

Ali, A., Ahmad, N., De Groot, E., Johannes Van Gerven, M. A., & Kietzmann, T. C. (2022). Predictive coding is a consequence of energy efficiency in recurrent neural networks. *Patterns*, *3*(12), 100639. https://doi.org/10.1016/j.patter.2022.100639

Alsop, D. C., Detre, J. A., Golay, X., Günther, M., Hendrikse, J., Hernandez-Garcia, L., Lu, H., MacIntosh, B. J., Parkes, L. M., Smits, M., van Osch, M. J. P., Wang, D. J. J., Wong, E. C., & Zaharchuk, G. (2015). Recommended implementation of arterial spin-labeled perfusion MRI for clinical applications: A consensus of the ISMRM perfusion study group and the European consortium for ASL in dementia: Recommended Implementation of ASL for Clinical Applications. *Magnetic Resonance in Medicine*, *73*(1), 102–116. https://doi.org/10.1002/mrm.25197

Bach, D. R., & Dolan, R. J. (2012). Knowing how much you don't know: A neural organization of uncertainty estimates. *Nature Reviews Neuroscience*, *13*(8), 572–586. https://doi.org/10.1038/nrn3289

Barber, T. W., Brockway, J. A., & Higgins, L. S. (1970). THE DENSITY OF TISSUES IN AND ABOUT THE HEAD. *Acta Neurologica Scandinavica*, *46*(1), 85–92. https://doi.org/10.1111/j.1600-0404.1970.tb05606.x

Bastos, A. M., Usrey, W. M., Adams, R. A., Mangun, G. R., Fries, P., & Friston, K. (2012). Canonical Microcircuits for Predictive Coding. *Neuron*, *76*(4), 695–711. https://doi.org/10.1016/j.neuron.2012.10.038

Batterink, L. J., Reber, P. J., Neville, H. J., & Paller, K. A. (2015). Implicit and explicit contributions to statistical learning. *Journal of Memory and Language*, *83*, 62–78. https://doi.org/10.1016/j.jml.2015.04.004

Baudrexel, S., Volz, S., Preibisch, C., Klein, J. C., Steinmetz, H., Hilker, R., & Deichmann, R. (2009). Rapid single-scan T2*-mapping using exponential excitation pulses and image-based correction for linear background gradients: T2* Mapping With Field Gradient Correction. *Magnetic Resonance in Medicine*, *62*(1), 263–268. https://doi.org/10.1002/mrm.21971

Beck, J. M., Ma, W. J., Pitkow, X., Latham, P. E., & Pouget, A. (2012). Not Noisy, Just Wrong: The Role of Suboptimal Inference in Behavioral Variability. *Neuron*, *74*(1), 30–39. https://doi.org/10.1016/j.neuron.2012.03.016

Beierholm, U., Rohe, T., Ferrari, A., Stegle, O., & Noppeney, U. (2020). Using the past to estimate sensory uncertainty. *eLife*, *9*, e54172. https://doi.org/10.7554/eLife.54172

Blockley, N. P., Griffeth, V. E. M., Simon, A. B., & Buxton, R. B. (2013). A review of calibrated blood oxygenation level-dependent (BOLD) methods for the measurement of task-induced changes in brain oxygen metabolism: A REVIEW OF CALIBRATED BOLD METHODS. *NMR in Biomedicine*, *26*(8), 987–1003. https://doi.org/10.1002/nbm.2847

Blockley, N. P., Griffeth, V. E. M., Simon, A. B., Dubowitz, D. J., & Buxton, R. B. (2015). Calibrating the BOLD response without administering gases: Comparison of hypercapnia calibration with calibration using an asymmetric spin echo. *NeuroImage*, *104*, 423–429. https://doi.org/10.1016/j.neuroimage.2014.09.061

Bounmy, T., Eger, E., & Meyniel, F. (2023). A characterization of the neural representation of confidence during probabilistic learning. *NeuroImage*, *268*, 119849. https://doi.org/10.1016/j.neuroimage.2022.119849

Boxermann, J.L., Schmainda, K.M., Weisskoff, R.M. (2006). Relative Cerebral Blood Volume Maps Corrected for Contrast Agent Extravasation Significantly Correlate with Glioma Tumor Grade, Whereas Uncorrected Maps Do Not. *Amercian Journal of Neuroradiology*, *27*(4), 859–867.

Brady, T., Konkle, T., Alvarez, G. A., & Oliva, A. (2008). Visual long-term memory has a massive storage capacity for object details. *Proceedings of the National Academy of Sciences*, *105*(38), 14325–14329. https://doi.org/10.1073/pnas.0803390105

Bridges, D., Pitiot, A., MacAskill, M. R., & Peirce, J. W. (2020). The timing mega-study: Comparing a range of experiment generators, both lab-based and online. *PeerJ*, *8*, e9414. https://doi.org/10.7717/peerj.9414

Bright, M. G., Croal, P. L., Blockley, N. P., & Bulte, D. P. (2019). Multiparametric measurement of cerebral physiology using calibrated fMRI. *NeuroImage*, *187*, 128–144. https://doi.org/10.1016/j.neuroimage.2017.12.049

Chalk, M., Marre, O., & Tkačik, G. (2018). Toward a unified theory of efficient, predictive, and sparse coding. *Proceedings of the National Academy of Sciences*, *115*(1), 186–191. https://doi.org/10.1073/pnas.1711114115

Christen, T., Schmiedeskamp, H., Straka, M., Bammer, R., & Zaharchuk, G. (2012). Measuring brain oxygenation in humans using a multiparametric quantitative blood oxygenation level dependent MRI approach. *Magnetic Resonance in Medicine*, *68*(3), 905–911. https://doi.org/10.1002/mrm.23283

Christie, S. T., & Schrater, P. (2015). Cognitive cost as dynamic allocation of energetic resources. *Frontiers in Neuroscience*, *9*. https://doi.org/10.3389/fnins.2015.00289

Clark, A. (2013). Whatever next? Predictive brains, situated agents, and the future of cognitive science. *Behavioral and Brain Sciences*, *36*(3), 181–204. https://doi.org/10.1017/S0140525X12000477

Commins, S. (2018). Efficiency: An underlying principle of learning? *Reviews in the Neurosciences*, *29*(2), 183–197. https://doi.org/10.1515/revneuro-2017-0050

Conway, C. M. (2020). How does the brain learn environmental structure? Ten core principles for understanding the neurocognitive mechanisms of statistical learning. *Neuroscience & Biobehavioral Reviews*, *112*, 279–299. https://doi.org/10.1016/j.neubiorev.2020.01.032

Dale, R., Duran, N., & Morehead, R. (2012). Prediction during statistical learning, and implications for the implicit/explicit divide. *Advances in Cognitive Psychology*, *8*(2), 196–209. https://doi.org/10.5709/acp-0115-z

de Lange, F. P., Heilbron, M., & Kok, P. (2018). How Do Expectations Shape Perception? *Trends in Cognitive Sciences*, *22*(9), 764–779. https://doi.org/10.1016/j.tics.2018.06.002

Devonshire, I. M., Papadakis, N. G., Port, M., Berwick, J., Kennerley, A. J., Mayhew, J. E. W., & Overton, P. G. (2012). Neurovascular coupling is brain region-dependent. *NeuroImage*, *59*(3), 1997–2006. https://doi.org/10.1016/j.neuroimage.2011.09.050

Dienel, G. A. (2014). Energy Metabolism of the Brain. In *From Molecules to Networks: An Introduction to Cellular and Molecular Neuroscience* (Third Edition, S. 53–117). Elsevier/Academic Press.

Drew, P. J. (2019). Vascular and neural basis of the BOLD signal. *Current Opinion in Neurobiology*, *58*, 61–69. https://doi.org/10.1016/j.conb.2019.06.004

Drew, P. J. (2022). Neurovascular coupling: Motive unknown. *Trends in Neurosciences*, *45*(11), 809–819. https://doi.org/10.1016/j.tins.2022.08.004

Feuerriegel, D., Vogels, R., & Kovács, G. (2021). Evaluating the evidence for expectation suppression in the visual system. *Neuroscience & Biobehavioral Reviews*, *126*, 368–381. https://doi.org/10.1016/j.neubiorev.2021.04.002

Feuerriegel, D., Yook, J., Quek, G. L., Hogendoorn, H., & Bode, S. (2021). Visual mismatch responses index surprise signalling but not expectation suppression. *Cortex*, *134*, 16–29. https://doi.org/10.1016/j.cortex.2020.10.006

Ficco, L., Mancuso, L., Manuello, J., Teneggi, A., Liloia, D., Duca, S., Costa, T., Kovacs, G. Z., & Cauda, F. (2021). Disentangling predictive processing in the brain: A meta-analytic study in favour of a predictive network. *Scientific Reports*, *11*(1), 16258. https://doi.org/10.1038/s41598-021-95603-5

Findling, C., Hubert, F., International Brain Laboratory, Acerbi, L., Benson, B., Benson, J., Birman, D., Bonacchi, N., Carandini, M., Catarino, J. A., Chapuis, G. A., Churchland, A. K., Dan, Y., DeWitt, E. E., Engel, T. A., Fabbri, M., Faulkner, M., Fiete, I. R., Freitas-Silva, L., … Pouget, A. (2023). *Brain-wide representations of prior information in mouse decision-making* [Preprint]. Neuroscience. https://doi.org/10.1101/2023.07.04.547684

Fiser, J., & Lengyel, G. (2022). Statistical Learning in Vision. *Annual Review of Vision Science*, *8*(1), 265–290. https://doi.org/10.1146/annurev-vision-100720-103343

Fox, P., Raichle, M., Mintun, M., & Dence, C. (1988). Nonoxidative glucose consumption during focal physiologic neural activity. *Science*, *241*(4864), 462–464. https://doi.org/10.1126/science.3260686

Friston, K. (2010). The free-energy principle: A unified brain theory? *Nature Reviews Neuroscience*, *11*(2), 127–138. https://doi.org/10.1038/nrn2787

Garcia, D. M., Duhamel, G., & Alsop, D. C. (2005). Efficiency of inversion pulses for background suppressed arterial spin labeling. *Magnetic Resonance in Medicine*, *54*(2), 366–372. https://doi.org/10.1002/mrm.20556

Geurts, L. S., Cooke, J. R. H., Van Bergen, R. S., & Jehee, J. F. M. (2022). Subjective confidence reflects representation of Bayesian probability in cortex. *Nature Human Behaviour*, *6*(2), 294–305. https://doi.org/10.1038/s41562-021-01247-w

Göttler, J., Kaczmarz, S., Kallmayer, M., Wustrow, I., Eckstein, H.-H., Zimmer, C., Sorg, C., Preibisch, C., & Hyder, F. (2019). Flow-metabolism uncoupling in patients with asymptomatic unilateral carotid artery stenosis assessed by multi-modal magnetic resonance imaging. *Journal of Cerebral Blood Flow & Metabolism*, *39*(11), 2132–2143. https://doi.org/10.1177/0271678X18783369

Griffeth, V. E. M., Simon, A. B., & Buxton, R. B. (2015). The coupling of cerebral blood flow and oxygen metabolism with brain activation is similar for simple and complex stimuli in human primary visual cortex. *NeuroImage*, *104*, 156–162. https://doi.org/10.1016/j.neuroimage.2014.10.003

Harris, J. J., Jolivet, R., & Attwell, D. (2012). Synaptic Energy Use and Supply. *Neuron*, *75*(5), 762–777. https://doi.org/10.1016/j.neuron.2012.08.019

Hedderich, D., Kluge, A., Pyka, T., Zimmer, C., Kirschke, J. S., Wiestler, B., & Preibisch, C. (2019). Consistency of normalized cerebral blood volume values in glioblastoma using different leakage correction algorithms on dynamic susceptibility contrast magnetic resonance imaging data without and with preload. *Journal of Neuroradiology*, *46*(1), 44–51. https://doi.org/10.1016/j.neurad.2018.04.006

Hirsch, N. M., & Preibisch, C. (2013). T2* Mapping with Background Gradient Correction Using Different Excitation Pulse Shapes. *American Journal of Neuroradiology*, *34*(6), E65–E68. https://doi.org/10.3174/ajnr.A3021

Hirsch, N. M., Toth, V., Förschler, A., Kooijman, H., Zimmer, C., & Preibisch, C. (2014). Technical considerations on the validity of blood oxygenation level-dependent-based MR assessment

of vascular deoxygenation: BOLD-BASED ASSESSMENT OF VASCULAR DEOXYGENATION. *NMR in Biomedicine*, *27*(7), 853–862. https://doi.org/10.1002/nbm.3131

Howarth, C., Gleeson, P., & Attwell, D. (2012). Updated energy budgets for neural computation in the neocortex and cerebellum. *Journal of Cerebral Blood Flow and Metabolism*, *32*(7), 1222–1232. https://doi.org/10.1038/jcbfm.2012.35

Huettel, S. A., Mack, P. B., & McCarthy, G. (2002). Perceiving patterns in random series: Dynamic processing of sequence in prefrontal cortex. *Nature Neuroscience*, *5*(5), 485–490. https://doi.org/10.1038/nn841

Hyder, D. S. F. (2010). Neurovascular and neurometabolic couplings in dynamic calibrated fMRI: transient oxidative neuroenergetics for block-design and event-related paradigms. *Frontiers in Neuroenergetics*, *2*. https://doi.org/10.3389/fnene.2010.00018

IT'IS Foundation. (2022). *Tissue Properties Database V4.1* [..Db, .xls, .txt, .pdf]. IT'IS Foundation. https://doi.org/10.13099/VIP21000-04-1

Kaczmarz, S., Hyder, F., & Preibisch, C. (2020). Oxygen extraction fraction mapping with multi-parametric quantitative BOLD MRI: Reduced transverse relaxation bias using 3D-GraSE imaging. *NeuroImage*, *220*, 117095. https://doi.org/10.1016/j.neuroimage.2020.117095

Kluge, A., Lukas, M., Toth, V., Pyka, T., Zimmer, C., & Preibisch, C. (2016). Analysis of three leakage-correction methods for DSC-based measurement of relative cerebral blood volume with respect to heterogeneity in human gliomas. *Magnetic Resonance Imaging*, *34*(4), 410–421. https://doi.org/10.1016/j.mri.2015.12.015

Knill, D. C., & Pouget, A. (2004). The Bayesian brain: The role of uncertainty in neural coding and computation. *Trends in Neurosciences*, *27*(12), 712–719. https://doi.org/10.1016/j.tins.2004.10.007

Koblinger, Á., Fiser, J., & Lengyel, M. (2021). Representations of uncertainty: Where art thou? *Current Opinion in Behavioral Sciences*, *38*, 150–162. https://doi.org/10.1016/j.cobeha.2021.03.009

Koller, M. (2016). robustlmm: An R Package for Robust Estimation of Linear Mixed-Effects Models. *Journal of Statistical Software*, *75*(6). https://doi.org/10.18637/jss.v075.i06

Lee, P., Chandel, N. S., & Simon, M. C. (2020). Cellular adaptation to hypoxia through hypoxia inducible factors and beyond. *Nature Reviews Molecular Cell Biology*, *21*(5), 268–283. https://doi.org/10.1038/s41580-020-0227-y

Leenders, K. L., Perani, D., Lammertsma, A. A., Heather, J. D., Buckingham, P., Jones, T., Healy, M. J. R., Gibbs, J. M., Wise, R. J. S., Hatazawa, J., Herold, S., Beaney, R. P., Brooks, D. J., Spinks, T., Rhodes, C., & Frackowiak, R. S. J. (1990). CEREBRAL BLOOD FLOW, BLOOD VOLUME AND OXYGEN UTILIZATION: NORMAL VALUES AND EFFECT OF AGE. *Brain*, *113*(1), 27–47. https://doi.org/10.1093/brain/113.1.27

Lin, A.-L., Fox, P. T., Hardies, J., Duong, T. Q., & Gao, J.-H. (2010). Nonlinear coupling between cerebral blood flow, oxygen consumption, and ATP production in human visual cortex. *Proceedings of the National Academy of Sciences*, *107*(18), 8446–8451. https://doi.org/10.1073/pnas.0909711107

Luczak, A., McNaughton, B. L., & Kubo, Y. (2022). Neurons learn by predicting future activity. *Nature Machine Intelligence*, *4*(1), 62–72. https://doi.org/10.1038/s42256-021-00430-y

Lüdecke, D., Ben-Shachar, M., Patil, I., Waggoner, P., & Makowski, D. (2021). performance: An R Package for Assessment, Comparison and Testing of Statistical Models. *Journal of Open Source Software*, *6*(60), 3139. https://doi.org/10.21105/joss.03139

Ma, W. J., & Jazayeri, M. (2014). Neural Coding of Uncertainty and Probability. *Annual Review of Neuroscience*, *37*(1), 205–220. https://doi.org/10.1146/annurev-neuro-071013-014017

Ma, Y., Sun, H., Cho, J., Mazerolle, E. L., Wang, Y., & Pike, G. B. (2020). Cerebral OEF quantification: A comparison study between quantitative susceptibility mapping and dual-gas calibrated BOLD imaging. *Magnetic Resonance in Medicine*, *83*(1), 68–82. https://doi.org/10.1002/mrm.27907

Maheu, M., Meyniel, F., & Dehaene, S. (2022). Rational arbitration between statistics and rules in human sequence processing. *Nature Human Behaviour*, *6*(8), 1087–1103. https://doi.org/10.1038/s41562-021-01259-6

Manahova, M. E., Mostert, P., Kok, P., Schoffelen, J.-M., & de Lange, F. P. (2018). Stimulus Familiarity and Expectation Jointly Modulate Neural Activity in the Visual Ventral Stream. *Journal of Cognitive Neuroscience*, *30*(9), 1366–1377. https://doi.org/10.1162/jocn_a_01281

Meyniel, F., & Dehaene, S. (2017). Brain networks for confidence weighting and hierarchical inference during probabilistic learning. *Proceedings of the National Academy of Sciences*, *114*(19). https://doi.org/10.1073/pnas.1615773114

Meyniel, F., Schlunegger, D., & Dehaene, S. (2015). The Sense of Confidence during Probabilistic Learning: A Normative Account. *PLOS Computational Biology*, *11*(6), e1004305. https://doi.org/10.1371/journal.pcbi.1004305

Meyniel, F., Sigman, M., & Mainen, Z. F. (2015). Confidence as Bayesian Probability: From Neural Origins to Behavior. *Neuron*, *88*(1), 78–92. https://doi.org/10.1016/j.neuron.2015.09.039

Moradi, F., Buračas, G. T., & Buxton, R. B. (2012). Attention strongly increases oxygen metabolic response to stimulus in primary visual cortex. *NeuroImage*, *59*(1), 601–607. https://doi.org/10.1016/j.neuroimage.2011.07.078

Moradi, F., & Buxton, R. B. (2013). Adaptation of cerebral oxygen metabolism and blood flow and modulation of neurovascular coupling with prolonged stimulation in human visual cortex. *NeuroImage*, *82*, 182–189. https://doi.org/10.1016/j.neuroimage.2013.05.110

Mutsaerts, H. J. M. M., Steketee, R. M. E., Heijtel, D. F. R., Kuijer, J. P. A., van Osch, M. J. P., Majoie, C. B. L. M., Smits, M., & Nederveen, A. J. (2014). Inter-Vendor Reproducibility of Pseudo-Continuous Arterial Spin Labeling at 3 Tesla. *PLoS ONE*, *9*(8), e104108. https://doi.org/10.1371/journal.pone.0104108

Noble, S., Curtiss, J., Pessoa, L., & Scheinost, D. (2023). *The tip of the iceberg: A call to embrace anti-localizationism in human neuroscience research*. PsyArXiv. https://doi.org/10.31234/osf.io/9eqh6

Noble, S., Mejia, A. F., Zalesky, A., & Scheinost, D. (2022). Improving power in functional magnetic resonance imaging by moving beyond cluster-level inference. *Proceedings of the National Academy of Sciences*, *119*(32), e2203020119. https://doi.org/10.1073/pnas.2203020119

Peirce, J., Gray, J. R., Simpson, S., MacAskill, M., Höchenberger, R., Sogo, H., Kastman, E., & Lindeløv, J. K. (2019). PsychoPy2: Experiments in behavior made easy. *Behavior Research Methods*, *51*(1), 195–203. https://doi.org/10.3758/s13428-018-01193-y

Pessoa, L. (2023). The Entangled Brain. *Journal of Cognitive Neuroscience*, 1–12. https://doi.org/10.1162/jocn_a_01908

Pouget, A., Drugowitsch, J., & Kepecs, A. (2016). Confidence and certainty: Distinct probabilistic quantities for different goals. *Nature Neuroscience*, *19*(3), 366–374. https://doi.org/10.1038/nn.4240

Quintela-López, T., Shiina, H., & Attwell, D. (2022). Neuronal energy use and brain evolution. *Current Biology*, *32*(12), R650–R655. https://doi.org/10.1016/j.cub.2022.02.005

Raichle, M. E., & Mintun, M. A. (2006). BRAIN WORK AND BRAIN IMAGING. *Annual Review of Neuroscience*, *29*(1), 449–476. https://doi.org/10.1146/annurev.neuro.29.051605.112819

Rao, R. P. N., & Ballard, D. H. (1999). Predictive coding in the visual cortex: A functional interpretation of some extra-classical receptive-field effects. *Nature Neuroscience*, *2*(1), 79–87. https://doi.org/10.1038/4580

Richter, D., Ekman, M., & de Lange, F. P. (2018). Suppressed Sensory Response to Predictable Object Stimuli throughout the Ventral Visual Stream. *The Journal of Neuroscience*, *38*(34), 7452–7461. https://doi.org/10.1523/JNEUROSCI.3421-17.2018

Roberts, J. A., Iyer, K. K., Vanhatalo, S., & Breakspear, M. (2014). Critical role for resource constraints in neural models. *Frontiers in Systems Neuroscience*, *8*. https://doi.org/10.3389/fnsys.2014.00154

Sanders, J. I., Hangya, B., & Kepecs, A. (2016). Signatures of a Statistical Computation in the Human Sense of Confidence. *Neuron*, *90*(3), 499–506. https://doi.org/10.1016/j.neuron.2016.03.025

Sauter, M., Draschkow, D., & Mack, W. (2020). Building, Hosting and Recruiting: A Brief Introduction to Running Behavioral Experiments Online. *Brain Sciences*, *10*(4), 251. https://doi.org/10.3390/brainsci10040251

Schaefer, A., Kong, R., Gordon, E. M., Laumann, T. O., Zuo, X.-N., Holmes, A. J., Eickhoff, S. B., & Yeo, B. T. T. (2018). Local-Global Parcellation of the Human Cerebral Cortex from Intrinsic Functional Connectivity MRI. *Cerebral Cortex*, *28*(9), 3095–3114. https://doi.org/10.1093/cercor/bhx179

Schapiro, A., & Turk-Browne, N. (2015). Statistical Learning. In *Brain Mapping* (S. 501–506). Elsevier. https://doi.org/10.1016/B978-0-12-397025-1.00276-1

Sengupta, B., Stemmler, M. B., & Friston, K. (2013). Information and Efficiency in the Nervous System—A Synthesis. *PLoS Computational Biology*, *9*(7), e1003157. https://doi.org/10.1371/journal.pcbi.1003157

Stefanics, G., Kimura, M., & Czigler, I. (2011). Visual Mismatch Negativity Reveals Automatic Detection of Sequential Regularity Violation. *Frontiers in Human Neuroscience*, *5*. https://doi.org/10.3389/fnhum.2011.00046

Teufel, C., & Fletcher, P. C. (2020). Forms of prediction in the nervous system. *Nature Reviews Neuroscience*, *21*(4), 231–242. https://doi.org/10.1038/s41583-020-0275-5

Theriault, J. E., Shaffer, C., Dienel, G. A., Sander, C. Y., Hooker, J. M., Dickerson, B. C., Barrett, L. F., & Quigley, K. S. (2023). A Functional Account of Stimulation-based Aerobic Glycolysis and its Role in Interpreting BOLD Signal Intensity Increases in Neuroimaging Experiments. *Neuroscience & Biobehavioral Reviews*, 105373. https://doi.org/10.1016/j.neubiorev.2023.105373

Turk-Browne, N. B., Jungé, J. A., & Scholl, B. J. (2005). The Automaticity of Visual Statistical Learning. *Journal of Experimental Psychology: General*, *134*(4), 552–564. https://doi.org/10.1037/0096-3445.134.4.552

Turk-Browne, N. B., Scholl, B. J., Chun, M. M., & Johnson, M. K. (2009). Neural Evidence of Statistical Learning: Efficient Detection of Visual Regularities Without Awareness. *Journal of Cognitive Neuroscience*, *21*(10), 1934–1945. https://doi.org/10.1162/jocn.2009.21131

Turk-Browne, N. B., Scholl, B. J., Johnson, M. K., & Chun, M. M. (2010). Implicit Perceptual Anticipation Triggered by Statistical Learning. *Journal of Neuroscience*, *30*(33), 11177–11187. https://doi.org/10.1523/JNEUROSCI.0858-10.2010

Vadillo, M. A., Konstantinidis, E., & Shanks, D. R. (2016). Underpowered samples, false negatives, and unconscious learning. *Psychonomic Bulletin & Review*, *23*(1), 87–102. https://doi.org/10.3758/s13423-015-0892-6

Walsh, K. S., McGovern, D. P., Clark, A., & O'Connell, R. G. (2020). Evaluating the neurophysiological evidence for predictive processing as a model of perception. *Annals of the New York Academy of Sciences*, *1464*(1), 242–268. https://doi.org/10.1111/nyas.14321

Warren, R. E., & Frier, B. M. (2005). Hypoglycaemia and cognitive function. *Diabetes, Obesity and Metabolism*, *7*(5), 493–503. https://doi.org/10.1111/j.1463-1326.2004.00421.x

Xu, F., Ge, Y., & Lu, H. (2009). Noninvasive quantification of whole-brain cerebral metabolic rate of oxygen ($CMRO_2$) by MRI: Quantification of $CMRO_2$. *Magnetic Resonance in Medicine*, *62*(1), 141–148. https://doi.org/10.1002/mrm.21994

Yablonskiy, D. A., & Haacke, E. M. (1994). Theory of NMR signal behavior in magnetically inhomogeneous tissues: The static dephasing regime. *Magnetic Resonance in Medicine*, *32*(6), 749–763. https://doi.org/10.1002/mrm.1910320610

Yon, D., & Frith, C. D. (2021). Precision and the Bayesian brain. *Current Biology*, *31*(17), R1026–R1032. https://doi.org/10.1016/j.cub.2021.07.044

Yu, L., & Yu, Y. (2017). Energy-efficient neural information processing in individual neurons and neuronal networks: Energy Efficiency in Neural Systems. *Journal of Neuroscience Research*, *95*(11), 2253–2266. https://doi.org/10.1002/jnr.24131

Zénon, A., Solopchuk, O., & Pezzulo, G. (2019). An information-theoretic perspective on the costs of cognition. *Neuropsychologia*, *123*, 5–18. https://doi.org/10.1016/j.neuropsychologia.2018.09.013

Zhou, D., Lynn, C. W., Cui, Z., Ciric, R., Baum, G. L., Moore, T. M., Roalf, D. R., Detre, J. A., Gur, R. C., Gur, R. E., Satterthwaite, T. D., & Bassett, D. S. (2022). Efficient coding in the economics of

human brain connectomics. *Network Neuroscience*, *6*(1), 234–274.

https://doi.org/10.1162/netn_a_00223